

# Fracture resistance via topology optimisation

V J Challis<sup>a</sup> A P Roberts<sup>a</sup> A H Wilkins<sup>a,\*</sup>

<sup>a</sup>*Department of Mathematics, University of Queensland, Brisbane, QLD 4072, Australia*

---

## Abstract

The fracture resistance of structures is optimised using the level-set method. Fracture resistance is assumed to be related to the elastic energy released by a crack propagating in a normal direction from parts of the boundary which are in tension, and is calculated using the virtual crack extension technique. The shape derivative of the fracture-resistance objective function is derived. Two illustrative two-dimensional case studies are presented: a hole in a plate subjected to biaxial strain; and a bridge fixed at both ends subjected to a single load in which the compliance and fracture resistance are jointly optimised. The structures obtained have rounded corners and more material at places where they are in tension. Based on the results, we propose that fracture resistance may be modelled more easily but less directly by including a term proportional to surface area in the objective function, in conjunction with non-linear elasticity where the Young's modulus in tension is lower than in compression.

*Key words:* Topology optimisation; Fracture; Level-set. 65K10 optimisation and variational techniques; 74R10 Brittle fracture; 74P10 optimisation of other properties; 74P15 Topological methods.

---

## 1 Introduction

Topology optimisation involves finding the geometry of an object which minimises an objective function, with no constraints on the object's topology [1]. Broadly speaking, there are currently two main methods for studying such problems: the homogenisation method and its variants such as the well-established

---

\* Corresponding author. Telephone: +61 7 3365 3266. Fax: +61 7 3365 1477

Email addresses: [vchallis@maths.uq.edu.au](mailto:vchallis@maths.uq.edu.au) (V J Challis), [apr@maths.uq.edu.au](mailto:apr@maths.uq.edu.au) (A P Roberts), [awilkins@maths.uq.edu.au](mailto:awilkins@maths.uq.edu.au) (A H Wilkins).

SIMP method [2, 3]; and, the level-set method [4]. In the former, the optimisation proceeds via a sequence of ‘fictitious’ materials which have properties unrealizable in nature until converging to the minimum containing only real materials [5–8]. In the latter, the process uses only real materials and moves boundaries to decrease the objective function at every iteration [9–12]. In its most naive implementation it typically converges slowly towards a *local* minimum, although recently some authors have proposed more sophisticated strategies to address these problems [13–24]. These strategies are not used here.

Topology optimisation has been used to study many problems, and in particular the elastic problem, where the objective function is the object’s compliance or total elastic energy for a particular set of external loads and boundary constraints, has been well studied. Bendsøe *et al.* [25] have prepared a recent review which discusses problems involving pressure loads, electromagnetic and acoustic wave propagation, fluid flow, articulated mechanisms and buckling.

Level-set methods were first applied to structural optimisation in [9] and have since been applied to problems in two and three dimensions including compliance minimisation with single and multiple load cases [11, 12, 14, 15, 17–23, 26–30], multi-material problems [27, 28, 30, 31], eigenfrequency problems [10, 19, 29], gripping and clamping devices [11, 15, 18, 19, 26, 27, 31], and shape and image reconstruction [13, 16].

The problem of optimising a material’s fracture toughness is addressed in this paper. Our definition of fracture toughness involves consideration of cracks propagating in a normal direction from any point on the object’s boundary into its interior. Thus, the level-set method is used since the objects of the intermediate iterations in the homogenisation/SIMP method have no well-defined “boundaries”, being solid masses of fictitious materials. The use of this method also removes the problem of defining the fracture toughness of fictitious materials.

The examples presented are two dimensional (2D). They are biphasic, consisting of “solid” which has a Young’s modulus of unity and a Poisson’s ratio of 0.3, and “void” which has a Young’s modulus of zero.

Our approach closely follows Allaire *et al.* and for brevity we do not reproduce their methodology, rather we refer readers to the article [11].

## 2 Brittle fracture and the objective function

According to the classic work of Griffith [32], a brittle material fractures if the elastic energy released upon crack propagation exceeds the material’s “fracture surface energy”, which is a material-specific quantity parameterising the strength of the intermolecular bonds [33]. Given this quantity, the maximum allowed load for a particular situation may be obtained by calculating the elastic energy released for all possible crack propagation paths. A crack can nucleate and propagate from within a material, or it may nucleate from its boundary and propagate inwards. The latter situation only is considered here.

The energy release rate for crack propagation may be calculated by finding the material’s elastic energy for two configurations differing only by a small change in crack length. In practice, where the two energies are calculated numerically, this is computationally costly, and for the linear elastic case methods exist which only require one elastic relaxation, such as (for 2D) the J-integral [34], or equivalently, the virtual crack extension method [35, 36].

Special cases of these methods may be interpreted as a particular shape derivatives as follows. Denote the domain occupied by the elastic material by  $\Omega$ . It has boundary  $\partial\Omega = \Gamma_N \cup \Gamma_D$  with outward unit normal  $n$ . The material is subjected to external tractions  $g$  on  $\Gamma_N$  (Neumann conditions), body forces  $f$  in its interior, and its boundary has fixed displacement,  $u^D$ , on  $\Gamma_D$  (Dirichlet conditions). The displacement field that solves this linear elastic problem is denoted by  $u_i$ , and denote the energy density by  $W$ :

$$W = \frac{1}{2} \nabla_i u_j A_{ijkl} \nabla_k u_l .$$

Here and below the indices  $i, j, k, l = (1, \dots, d)$  in  $d$  dimensions, summation over repeated indices is implied, the index  $n$  is reserved for the “normal direction” (e.g.  $x_n = x_i n_i$  for any vector  $x$ ), and  $\nabla_i$  is the derivative, so the strain is  $\frac{1}{2}(\nabla_i u_j + \nabla_j u_i)$ . The elastic tensor is denoted by  $A_{ijkl}$ . The compliance is

$$C = \int_{\Omega} f_i u_i + \int_{\Gamma_N} g_i u_i . \tag{1}$$

Consider deforming the material (coordinatised by  $x$ ) with the diffeomorphism

$$x \rightarrow x + \theta(x) .$$

Classical results [11, 37–39] give the compliance change as a function of  $\theta$  as

$$\begin{aligned}
C'(\theta) = & 2 \int_{\Gamma_N} \theta \cdot n (\nabla_n(g \cdot u) + Hg \cdot u - W) \\
& + 2 \int_{\Gamma_D} \theta \cdot n (\nabla_n(u_j - u_j^D) A_{njk} \nabla_k u_l - W) .
\end{aligned} \tag{2}$$

In this formula  $\nabla_n$  denotes the derivative in the normal direction and  $H = \nabla \cdot n$  is the mean curvature of the boundary.

To make the connection with the J-integral and virtual crack extension, consider the two dimensional (2D) case. Parameterise length along the boundary by  $y$ . (The boundary may consist of disjoint pieces, but that is irrelevant because of the following assumption.) Assume that  $\theta$  takes the form

$$-\theta \cdot n = \epsilon k_0(y) = \begin{cases} \epsilon(\delta + y) & \text{for } -\delta \leq y \leq 0 \\ \epsilon(\delta - y) & \text{for } 0 \leq y \leq \delta \\ 0 & \text{otherwise} \end{cases} \quad \text{on } \partial\Omega. \tag{3}$$

Here  $\epsilon$  is a small number parameterising the “depth” of the boundary perturbation, and  $\delta$  parameterises the “length” of the perturbation with  $\delta \gg \epsilon$ . The perturbation is shown in Fig. 1. The subscript on  $k$  indicates that the

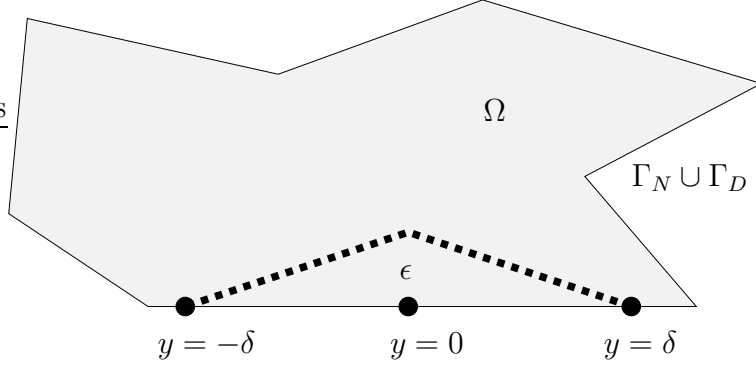


Fig. 1. The perturbation of the boundary given by Eq. (3).

perturbation is rooted at  $y = 0$ , and suppose that  $y = 0$  is part of  $\Gamma_N$ . This is exactly a particular “virtual crack extension”: in a finite element scheme the point  $y = 0$  is one node of the finite element mesh,  $k_0$  corresponds to the virtual movement of this single node while keeping all other nodes fixed. Specialising Eq. (2) to this case gives

$$C'(\theta) = \int dy \epsilon k_0(y) (W - \nabla_n(g \cdot u) - Hg \cdot u) . \tag{4}$$

When the section of boundary  $-\delta \leq y \leq \delta$  is straight,  $H = 0$ , and this expression may be compared with Rice’s J-integral evaluated along a contour

close to the point  $y = 0$ .

In standard fracture situations where the material contains a well-defined crack of interest, numerical errors in the elasticity solution mean it is more accurate to move all the nodes which lie in the vicinity of a crack tip —  $k$  has nonzero support at all of these nodes — in order to calculate the energy release rate (or compliance change) for crack propagation in a certain direction. Similarly, for well-defined straight cracks, errors can be minimised by evaluating the J-integral around a contour that is distant from the crack tip. In the current application, however, generically there will be no well-defined cracks, and so the movement of just one node is considered, corresponding to a small crack initiating and propagating from the boundary in the normal direction.

Motivated by these arguments, the objective function for fracture resistance considered here is

$$J_q = \int_{p \in S_+} k_p G^q \quad \text{where} \quad G = W - \nabla_n(g \cdot u) - Hg \cdot u . \quad (5)$$

The short-hand notation,  $G$ , has been introduced. The set  $S_+$  is all the points on  $\Gamma_N$  where the surface tension is positive, so as to exclude points of high compressive energies which may not actually lead to fracture. Further comments on this point are made in Sec. 8. An explicit restriction to  $\Gamma_N$  has been made, since the material is fixed at  $\Gamma_D$  so that part of the boundary cannot be moved, so its fracture resistance cannot be optimised. When the exponent,  $q$ , is large, minimising  $J_q$  corresponds to focussing on those few boundary points where the fracture resistance is low, while smaller  $q$  (say  $q = 1$ ) considers points in  $S_+$  more equally. The latter approach has been found to lead to more rapid convergence of the numerical algorithm, since the ‘special points’ in the former tend to move around during optimisation.

### 3 The shape derivative of the objective function

The shape derivative of the objective function is needed to implement the level-set scheme as detailed in Allaire *et al.* [11], since the velocity in the Hamilton-Jacobi (HJ) equation is the negative of the integrand of the shape derivative.

To find the shape derivative of Eq. (5), the formal method discussed in [11] and attributed to Céa [40] is used. The idea is to find a Lagrangian,  $L$ , which generates the equations of motion for the field(s) and reduces to the objective function when the fields satisfy their equations of motion (“on shell”). Because

of the former property, the derivative  $\delta L/\delta \text{fields} = 0$  on shell, so the shape derivative  $dL/d\Omega$  can be computed at fixed fields.

The elasticity problem is defined through the equations of motion

$$\begin{aligned} \nabla_j (A_{ijkl} \nabla_k u_l) &= -f_i \quad \text{in } \Omega, \\ A_{njk} \nabla_k u_l &= g_j \quad \text{on } \Gamma_N, \\ u_i &= u_i^D \quad \text{on } \Gamma_D. \end{aligned} \quad (6)$$

Written in terms of stress,  $\sigma$ , the first is simply  $\nabla_j \sigma_{ij} = -f_i$  and the second is  $\sigma_{nj} = g_j$ , so  $f$  is a body force and  $g$  a boundary traction.

There are many Lagrangians which generate these equations of motion, and the following contains just one auxiliary field  $M$  which is a Lagrange multiplier:

$$\begin{aligned} L_M = \int_{\Omega} \nabla_i M_j A_{ijkl} \nabla_k u_l - \int_{\Omega} M_i f_i - \int_{\Gamma_N} M_i g_i \\ - \int_{\Gamma_D} [M_j A_{njk} \nabla_k u_l + (u_j - u_j^D) A_{njk} \nabla_k M_l]. \end{aligned} \quad (7)$$

Varying  $M_i$  gives the correct equations of motion for  $u$ ; and

$$L_M = 0,$$

on shell.

Therefore, the Lagrangian

$$L = J_q + L_M,$$

satisfies the requirements given above. Varying  $u$  in this Lagrangian gives the equations of motion for the auxiliary field:

$$\begin{aligned} \nabla_j (A_{ijkl} \nabla_k M_l) &= 0 \quad \text{in } \Omega, \\ A_{njk} \nabla_k M_l &= \nabla_i^t (k_p q G^{q-1} A_{ijkl} \nabla_k u_l) + k_p q G^{q-1} (\nabla_n g_j + H g_j) \quad \text{on } \Gamma_N, \\ M_i &= 0 \quad \text{on } \Gamma_D. \end{aligned} \quad (8)$$

The derivative  $\nabla_i^t$  acts in the tangent plane only:

$$\nabla_i^t = \nabla_i - n_i \nabla_n.$$

In deriving these equations, the boundary conditions on  $u$  have been used, and it is assumed that  $k_p$  has zero support on  $\partial\Gamma_N$ , so that there is no boundary term when integrating by parts with the operator  $\nabla_i^t$ . These equations therefore define an elasticity problem with zero displacement on  $\Gamma_D$  and tractions applied to the boundary around the points  $p \in S_+$ .

Using the standard formulae found in [11], and evaluating on-shell (so that  $u = u^D$  and  $M = 0$  on  $\Gamma_D$ , for instance), the shape derivative of the objective function is

$$\begin{aligned} J'_q(\theta) = & \int_{S_+} (\nabla_n (k_p G^q) + H k_p G^q) \theta \cdot n + \int_{\partial\Omega} \nabla_i M_j A_{ijkl} \nabla_k u_l \theta \cdot n \\ & - \int_{\Gamma_N} (\nabla_n (g \cdot M) + H g \cdot M) \theta \cdot n \\ & - \int_{\Gamma_D} (\nabla_n M_j A_{njk} \nabla_k u_l + \nabla_n u_j A_{njk} \nabla_k M_l) \theta \cdot n. \end{aligned} \quad (9)$$

#### 4 Compliance minimisation and the volume or area constraint

In addition to fracture resistance, compliance minimisation is also considered in the examples below. The objective function used is

$$J = (1 - \lambda)C + \lambda J_q, \quad (10)$$

where  $\lambda$  is a fixed weighting factor. Both  $C$  and  $J_q$  are minimised when the material has infinite volume (3D) or area (2D). To avoid this, a maximum volume (3D) or area (2D),  $V_{\max}$ , is introduced, and the problem to be solved is

$$\text{Minimise } J \text{ subject to } \int_{\Omega} 1 \leq V_{\max}. \quad (11)$$

It is common in the literature to add a term proportional to the volume (or area) to the objective function, so the problem becomes: minimise a linear combination of  $J$  and volume (or area). Unfortunately this does not allow direct comparison of structures with different  $\lambda$  since altering  $\lambda$  will also produce different volume fractions. The problem stated in Eq. (11) does allow a direct comparison.

## 5 Finite element implementation

The finite element method is implemented using bi-linear (in 2D) square elements, as described in [41–43]. The original ( $u$ ) elastic problem is solved, and  $G$  at each boundary node is calculated to find the boundary tractions for the auxiliary ( $M$ ) problem. Four geometric arrangements are possible, as illustrated in Fig. 2. In the case of Fig. 2(a), the integral becomes

$$\int k_p G^q = \int_{-\delta}^0 dy k_0(G_{22}^q - G_{21}^q)_{x=0} + \int_0^\delta dy k_0(G_{12}^q - G_{11}^q)_{x=0}, \quad (12)$$

where the subscripts 11, etc, correspond to the values in the elements defined in Fig. 2. In calculating these  $G$  values,  $H = 0$  since the boundary is straight, and in the case illustrated  $G_{11} = 0 = G_{21}$ . In principle, if there is a boundary traction,  $g_i$ , acting at the central node then its action gets split over the elements 12 and 22 at  $y = 0$  (however, in the practical situations considered here and elsewhere the boundary never moves away from such a point so the point may be simply excluded from  $S_+$ ).

In the case of Fig. 2(b) and (c) the normal is taken to be  $(-1, -1)/\sqrt{2}$  to ascertain whether the point is in  $S_+$ . Algorithmically it is convenient to use the sum of two orthogonal virtual crack extensions as indicated in the figure, each with a similar expression to Eq. (12). In the case of Fig. 2(d), the normal direction is not well-defined. In this case, the two normal virtual crack extensions are tried (each can be decomposed into two orthogonal parts as in (b) and (c)), and the maximum of the two results (which will be numerically similar) is chosen.

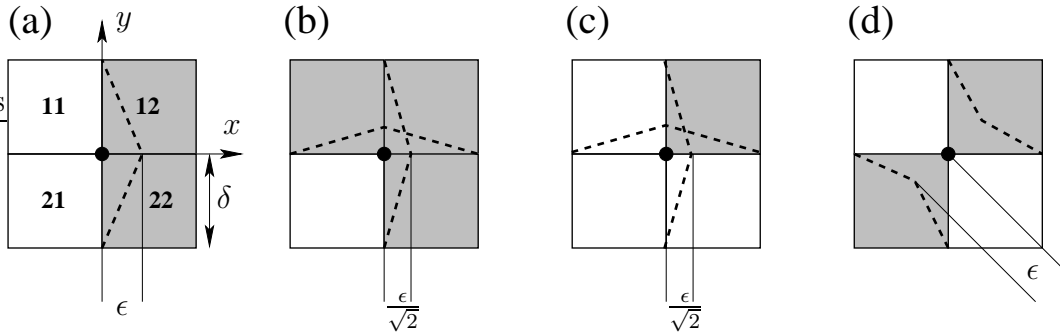


Fig. 2. Four possibilities for a node (black dot) on the boundary. (a): there are two neighbouring solid elements and two void elements. (b): three solid elements. (c): one solid element. (d): two diagonally-opposite solid elements. Virtual crack extensions for each are shown by dotted lines: (b), (c) and (d) can be decomposed into a linear combination of two orthogonal extensions. The surrounding elements are labelled 11, 12, 21 and 22 as shown in (a).

The elasticity problem is then solved for  $M$ . The surface tractions are applied at each point  $p \in S_+$  and its two neighbouring nodes on the boundary. A finite difference scheme is adopted to find the tangential divergence in Eq. (8):  $k_p q G^{q-1} \sigma_{ij}$  is evaluated at points half way between the nodes ( $y = \pm\delta/2$  with  $x = 0$  in Fig. 2(a)) and the appropriate differences taken. Cases Fig. 2(b), (c) and (d) follow similarly, for instance, in case (b)

$$\begin{aligned} \nabla_i^t k_0 q G^{q-1} \sigma_{ij} \Big|_{x=0=y} &= \frac{1}{\delta/\sqrt{2}} \left( k_0 q G^{q-1} \frac{(\sigma_{1j} - \sigma_{2j})}{\sqrt{2}} \Big|_{x=-\delta/2, y=0} \right. \\ &\quad \left. - k_0 q G^{q-1} \frac{(\sigma_{1j} - \sigma_{2j})}{\sqrt{2}} \Big|_{x=0, y=-\delta/2} \right) \end{aligned}$$

since the tangential stress is  $(\sigma_{1j} - \sigma_{2j})/\sqrt{2}$  and the distance between the points  $(-\delta/2, 0)$  and  $(0, -\delta/2)$  is  $\delta/\sqrt{2}$ .

After the elasticity problem for  $M$  has been solved, the shape derivative of  $J_q$  can be found by straightforward evaluation. The only nontrivial term in Eq (9) is  $\nabla_n (k_p G^q)$ . For Fig. 2(a), this is evaluated by taking the finite difference of Eq. (12) at  $x = 1$  (using a Young's modulus of zero for the 12 and 22 elements in the virtual crack extension calculation) with that at  $x = 0$ . Similar constructions are used for the other 3 cases in Fig. 2.

The void material has zero Young's modulus and thus the integrand of the shape derivative is zero for void elements. Consequently, the velocity,  $v$ , of the HJ evolution is zero too, and so the boundaries of the object will never move! Allaire *et al.* [11] promote the use of a so-called ersatz material, where the voids have a small nonzero Young's modulus, allowing the velocity to be extended into the void elements. This is not suitable here, since the first and third terms of Eq. (9) are only *defined* on the boundary. Therefore, a smoothing operation is performed as follows. The first and third terms are defined at the *nodal* points, so their contribution is spread equally to the four neighbouring elements. The second is evaluated at the midpoints of each of the solid elements, and then spread to the neighbours by the correlation:

$$v_{\text{new}}(i, j) = (2v(i, j) + v(i-1, j) + v(i+1, j) + v(i, j-1) + v(i, j+1))/6 .$$

This smoothing of the boundary values into the void allows the boundary to move during HJ evolution.

As found by other authors, the objective function typically decreases with each HJ iteration, only increasing when the solid volume fraction exceeds  $V_{\max}$ . When that occurs, the material is eroded away using a constant velocity in the HJ evolution until the volume fraction is  $0.99V_{\max}$ . The behaviour of  $J_q$  is not

as controlled as in the compliance-minimisation case because sometimes the movement of one part of the boundary causes  $G$  to increase markedly somewhere else. This may be seen in Fig. 6. Because our finite-element program is parallelised and hence rather quick, we evolve very slowly: each iteration involves an elastic relaxation and movement of the boundary by only *one* element.

## 6 Case study 1: the hole

The fracture resistance of a plate containing an arbitrarily shaped central hole must be maximised under the conditions that the hole area fraction is  $1/8$  and the plate is under uniform biaxial strain. This problem may be solved using  $\lambda = 1$  and  $V_{\max} = 7/8$ . Fig. 3 shows one initial condition, and the geometry at the minimum, which has a circular hole. Because this is the expected result, this case study illustrates that the algorithm is indeed maximising fracture resistance.

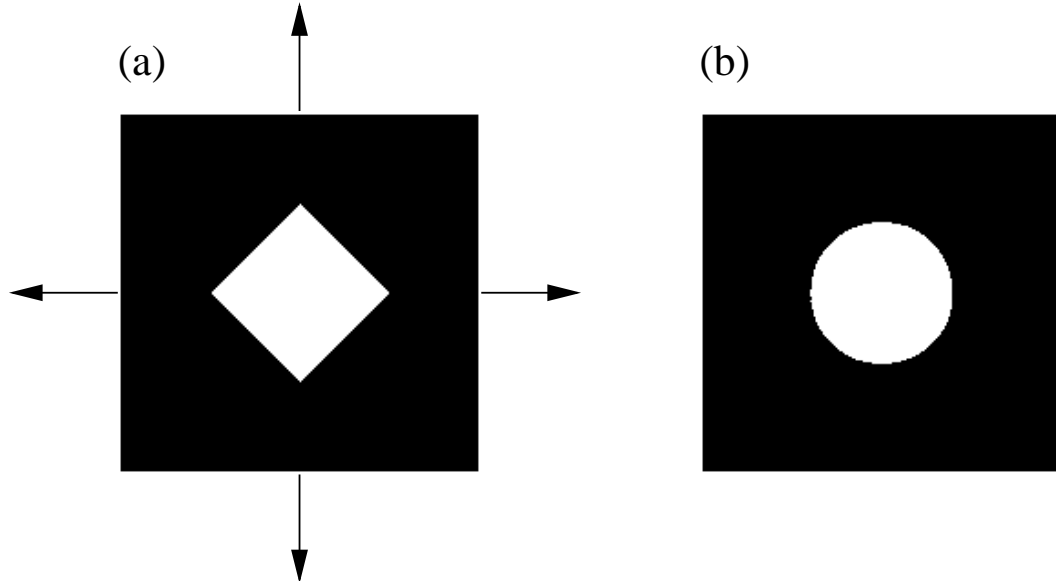


Fig. 3. (a): An initial configuration with  $J_2 = 973$ . (b) The minimum at  $J_2 = 177$ . This example has  $200 \times 200$  pixels.

## 7 Case study 2: the bridge

The ‘bridge’ problem is specified in Fig. 4 which also shows its solution for  $\lambda = 0$ ,  $V_{\max} = 17.1\%$ , and the length variable being twice the height. Similar problems were studied in [1, 11, 12, 14, 15, 18, 21, 22]. The compliance of the

structure shown in Fig. 4(b) is  $C = 26.5$ . This topology and geometry is also obtained using the SIMP method [1]. The simulations were performed on a  $200 \times 100$  mesh. A large variety of initial configurations were used in order to address the problem of converging to a local minimum, rather than a global one.

The minimum structure at  $\lambda = 0$  has  $J_1 = 0.5$  — 50 times less than  $C$  — so to weight fracture resistance meaningfully a value of  $\lambda \approx 1$  must be used. The following study considers the extreme case of  $\lambda = 1 - 10^{-5}$ . Less extreme values produce geometries that interpolate between the one shown here and the  $\lambda = 0$  case. In order to keep the structure within the rectangular domain of interest, it is assumed that any parts of the bridge on the bottom boundary are infinitely fracture resistant, otherwise the optimisation results in material enveloping the point of application of the load.

Figure 5 shows the optimal geometry, and Fig. 6 shows the objective function. This geometry has  $C = 34.3$ ,  $J_1 = 0.222$  and so  $J = 0.222$ . The following points may be noticed.

- (1) The parts of the structure which are in tension capture material from those in compression.
- (2) Corners are typically more rounded.
- (3) In the case of the bridge, the optimal topology is unchanged. In other cases that have been investigated (such as the cantilever), this is sometimes not true since a thin strut in compression can disappear entirely.
- (4)  $G$  is fairly constant over the parts of the boundary that are in tension, as shown in Fig. 7. This suggests that very similar geometries are obtained for  $q > 1$  (although the value of  $\lambda$  must also be scaled to obtain exactly the same geometry).

These points are supported by further simulations with different  $q$  and  $\lambda$ : because the structures obtained are actually quite similar we resist reproducing further graphics for brevity.

## 8 Discussion

In this paper fracture resistance has been defined through a virtual crack extension in a normal direction on parts of the boundary that are in tension. Because the normal stresses are typically close to zero on the boundary (even considering the few places where  $g \neq 0$ , discretisation effects and numerical errors which all yield nonzero normal stresses), the objective function for fracture resistance is close to an integral of the energy density over parts of the boundary,  $S_+$ , which are in tension.

If this restriction to  $S_+$  was removed, we propose that the the objective function for fracture resistance may be well approximated by a *surface integral* of the energy density, and therefore, when used in linear combination with the objective function for compliance, which is an integral of the energy density over the *volume* of the material, may be further replaced by an objective function proportional to the *surface area* (in 3D) or *perimeter* (in 2D). This provides a physical motivation for using a surface area or perimeter constraint/objective function, which are typically employed to penalise micro-fine structures sometimes encountered in structural optimisation problems.

The problem is more complicated with the restriction to  $S_+$ , as material is captured by the parts in tension. Those parts do not necessarily decrease significantly in surface area, but because they are more massive will have significantly less surface energy. Our experience is that in most cases the optimal topology does not change compared with the compliance-only situation, although the geometry may be significantly altered, as can be seen in Fig. 5. Similarly to above, we propose that this case may be modelled less directly, but probably more easily by including a term proportional to the surface area or perimeter in the objective function, in conjunction with using a non-linear elasticity law where the Young's modulus in tension is lower than in compression.

## 9 Acknowledgements

This work was supported by a grant from the Australian Research Council through the Discovery Grant scheme, and an Australian Postgraduate Award.

## References

- [1] M. P. Bendsøe, O. Sigmund, *Topology Optimization*, 2nd Edition, Springer, Berlin, 2004.
- [2] M. P. Bendsøe, N. Kikuchi, Generating optimal topologies in structural design using a homogenization method, *Comput. Methods Appl. Mech. Engng.* 71 (1988) 197–224.
- [3] M. P. Bendsøe, Optimal shape design as a material distribution problem, *Struct. Opt.* 1 (1989) 193–202.
- [4] S. J. Osher, J. A. Sethian, Fronts propagating with curvature dependent speed: Algorithms based on the Hamilton–Jacobi formulation, *J. Comput. Phys.* 79 (1988) 12–49.

- [5] K. Suzuki, N. Kikuchi, A homogenization method for shape and topology optimization, *Comp. Meth. Appl. Mechs. Engng.* 93 (1991) 291–318.
- [6] G. Allaire, E. Bonnetier, G. Francfort, F. Jouve, Shape optimization by the homogenization method, *Numerische Mathematik* 76 (1997) 27–68.
- [7] M. P. Bendsøe, O. Sigmund, Material interpolations in topology optimization, *Archive of Applied Mechanics* 69 (1999) 635–654.
- [8] G. Allaire, Shape optimization by the homogenization method, Springer Verlag, New York, 2001.
- [9] J. A. Sethian, A. Wiegmann, Structural boundary design via level set and immersed interface methods, *J. Comput. Phys.* 163 (2) (2000) 489–528.
- [10] S. J. Osher, F. Santosa, Level set methods for optimization problems involving geometry and constraints I. frequencies of a two-density inhomogeneous drum, *J. Comput. Phys.* 171 (2001) 272–288.
- [11] G. Allaire, F. Jouve, A.-M. Toader, Structural optimization using sensitivity analysis and a level-set method, *J. Comput. Phys.* 194 (2004) 363–393.
- [12] M. Y. Wang, X. Wang, D. Guo, A level set method for structural topology optimization, *Comput. Meth. Appl. Mech. Engrg.* 192 (2003) 227–246.
- [13] M. Burger, B. Hackl, W. Ring, Incorporating topological derivatives into level set methods, *J. Comput. Phys.* 194 (2004) 334–362.
- [14] X. Wang, M. Y. Wang, D. Guo, Structural shape and topology optimization in a level-set-based framework of region representation, *Struct. Multidisc. Optim.* 27 (2004) 1–19.
- [15] G. Allaire, F. de Gournay, F. Jouve, A.-M. Toader, Structural optimization using topological and shape sensitivity via a level set method, *Control and Cybernetics* 34 (1) (2005) 59–80.
- [16] M. Hintermüller, Fast level set algorithms using shape and topological sensitivity information, *Control and Cybernetics* 34 (2005) 305–324.
- [17] X. Guo, K. Zhao, M. Y. Wang, A new approach for simultaneous shape and topology optimization based on dynamic implicit surface function, *Control and Cybernetics* 34 (1) (2005) 255–282.
- [18] S. Amstutz, H. Andrä, A new algorithm for topology optimization using a level-set method, *J. Comput. Phys.* 216 (2006) 573–588.
- [19] F. de Gournay, Velocity extension for the level-set method and multiple eigenvalues in shape optimization, *SIAM J Control and Optimization* 45 (2006) 343–367.
- [20] A. A. Gomes, A. Suleiman, Application of spectral level set methodology in topology optimization, *Structural and Multidisciplinary Optimization* (2006) doi:10.1007/s00158-006-0005-2.

- [21] S. Wang, M. Y. Wang, A moving superimposed finite element method for structural topology optimization, *Int. J. Numer. Methods Eng.* 65 (2006) 1892–1922.
- [22] S. Wang, M. Y. Wang, Radial basis functions and level set method for structural topology optimization, *Int. J. Num. Methods Engng.* 65 (2006) 2060–2090.
- [23] S. Y. Wang, M. Y. Wang, Structural shape and topology optimization using an implicit free boundary parameterization method, *Computer Modelling in Engineering and Sciences* 13 (2) (2006) 119–147.
- [24] D. N. Wilke, S. Kok, A. A. Groenwold, A quadratically convergent unstructured remeshing strategy for shape optimization, *Int. J. Numer. Meth. Eng.* 65 (2006) 1–17.
- [25] M. P. Bendsøe, E. Lund, N. Olhoff, Topology optimization — broadening the areas of application, *Control and Cybernetics* 34 (1) (2005) 7–35.
- [26] G. Allaire, F. Jouve, A.-M. Toader, A level-set method for shape optimization, *C. R. Acad. Sci. Paris Série I* 334 (2002) 1125–1130.
- [27] M. Yulin, W. Xiaoming, A level set method for structural topology optimization and its applications, *Adv. Eng. Software* 35 (2004) 415–441.
- [28] M. Wang, X. Wang, “color” level sets: a multi-phase method for structural topology optimization with multiple materials, *Comput. Methods Appl. Mech. Engng.* 193 (2004) 469–496.
- [29] G. Allaire, F. Jouve, A level-set method for vibration and multiple loads structural optimization, *Comput. Methods Appl. Mech. Engng.* 194 (2005) 3269–3290.
- [30] M. Y. Wang, X. Wang, A level-set based variational method for design and optimization of heterogeneous objects, *Computer-Aided Design* 37 (2005) 321–337.
- [31] M. Y. Wang, S. K. Chen, X. M. Wang, Y. L. Mei, Design of multimaterial compliant mechanisms using level-set methods, *Journal of Mechanical Design* 127 (2005) 941–956.
- [32] A. A. Griffith, The phenomena of rupture and flow in solids, *Phil. Trans. R. Soc. (Lond.) A221* (1921) 163–198.
- [33] B. R. Lawn, *Fracture of brittle solids*, 2nd Edition, Cambridge University Press, Cambridge, UK, 1993.
- [34] J. R. Rice, A path independent integral and the approximate analysis of strain concentration by notches and cracks, *J. Appl. Mech.* 35 (1968) 379–386.
- [35] D. M. Parks, A stiffness derivative finite element technique for determination of crack tip stress intensity factors, *Int. J. Fract.* 10 (1974) 487–502.
- [36] T. K. Hellen, On the method of virtual crack extensions, *Int. J. Numer. Methods Engng.* 9 (1975) 187–207.

- [37] F. Murat, S. Simon, Etudes de problèmes d'optimal design, Vol. 41 of Lecture Notes in Computer Science, Springer Verlag, Berlin, 1976.
- [38] J. Simmon, Differentiation with respect to the domain in boundary value problems, *Numer. Funct. Anal. Optim.* 2 (1980) 649–687.
- [39] J. Sokołowski, J. P. Zolesio, Introduction to shape optimization: shape sensitivity analysis, Vol. 10 of Springer Series in Computational Mathematics, Springer, Berlin, 1992.
- [40] J. Céa, Conception optimale ou identification de formes, calcul raide de la dérivée directionnelle de la fonction coût, *Math. Model. Numer. Anal.* 20 (1986) 371–402.
- [41] E. J. Garboczi, A. R. Day, An algorithm for computing the effective linear elastic properties of heterogeneous materials: three-dimensional results for composites with equal phase poisson ratios, *J. Mech. Phys. Solids* 43 (1995) 1349–1362.
- [42] E. J. Garboczi, Finite element and finite difference programs for computing the linear electric and elastic properties of digital images of random materials, Tech. rep., NISTIR 6269 (1998).  
URL <http://ciks.cbt.nist.gov/garbocz/manual/man.html>
- [43] A. J. Roberts, A. H. Wilkins, A simple, versatile finite element method for fracture in heterogeneous materials, Submitted to *J. Comput. Phys.*

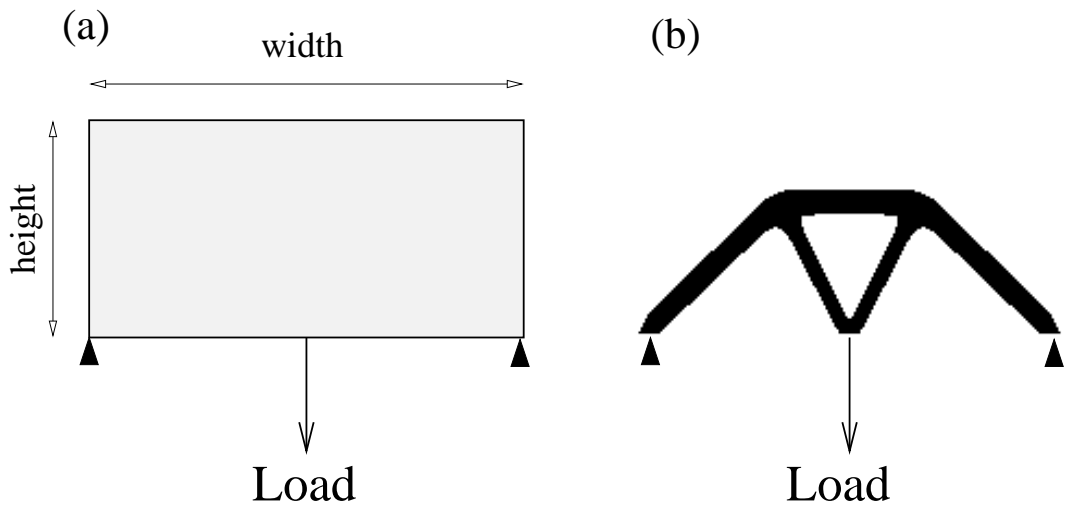


Fig. 4. (a): The bridge problem has two points with fixed zero displacement and a single load. (b): The solution for width =  $2 \times$  height,  $V_{\max} = 17.1\%$  and  $\lambda = 0$ .



Fig. 5. Left: The optimal geometry for the bridge problem for  $\lambda = 1 - 10^{-6}$ . Right: a comparison of the left-hand structure and the optimal geometry for  $\lambda = 0$ .

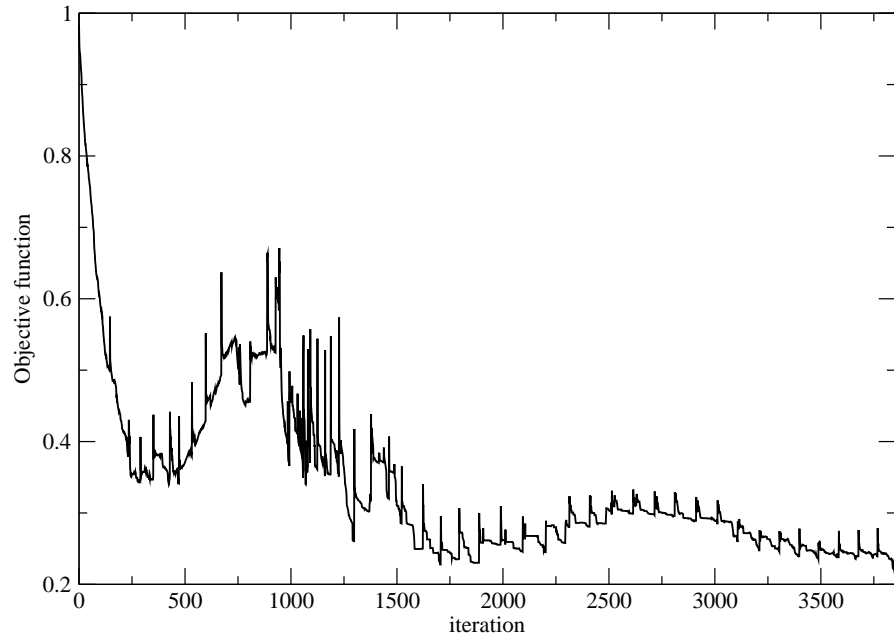


Fig. 6. The objective function at each iteration for the bridge case study. Each iteration involves either: adding *two* elements (symmetrically about the symmetry axis) to the solid structure; or, eroding the structure so that the solid volume fraction is  $0.99V_{\max}$ . The latter causes large jumps while the former typically decreases  $J$ , as discussed in the text. The initial configuration had topology and geometry similar to that of the compliance-optimised solution of Fig. 4(b).

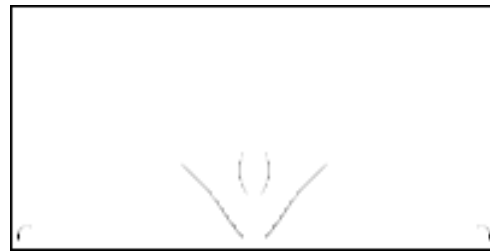


Fig. 7. Greyscaling indicating the value of  $G$  for each boundary node in the optimal solution shown in Fig. 5. Dark regions, such as those close to the supporting points indicate high  $G$ , lighter regions indicate lower  $G$ .